High-resolution satellite data reveal an increase in peak growing season gross primary production in a high-Arctic wet tundra ecosystem 1992-2008

Tagesson, Torbern; Mastepanov, Mikhail; Tamstorf, Mikkel P.; Eklundh, Lars; Schubert, Per; Ekberg, Anna; Sigsgaard, Charlotte; Christensen, Torben; Ström, Lena

Published in:
International Journal of Applied Earth Observation and Geoinformation

DOI:
10.1016/j.jag.2012.03.016

2012

Document Version:
Publisher's PDF, also known as Version of record

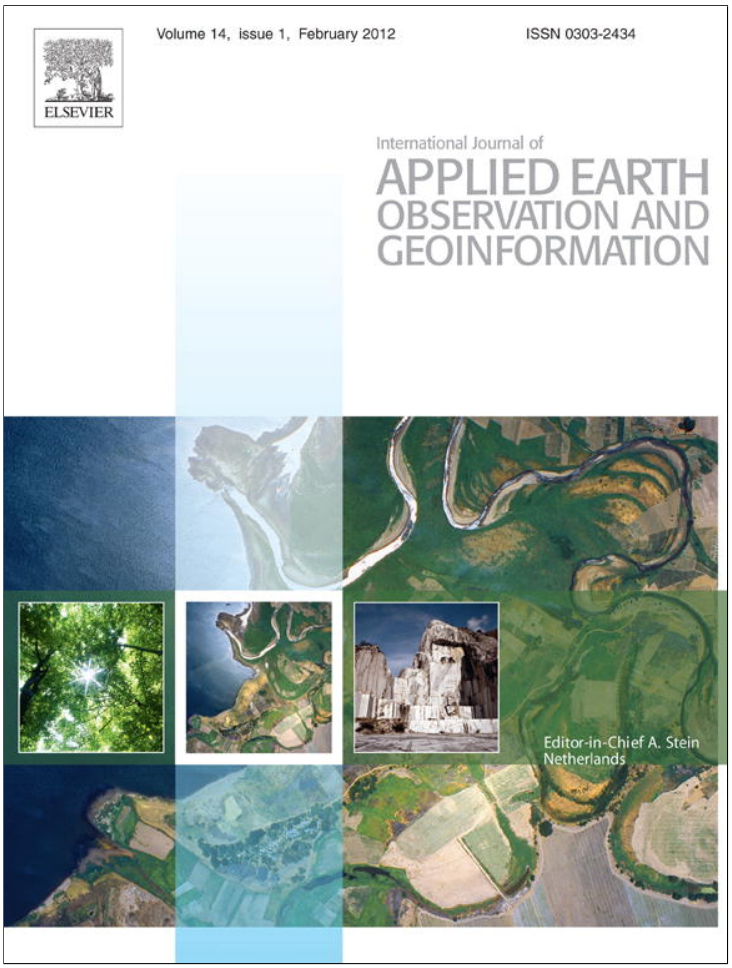

(This is a sample cover image for this issue. The actual cover is not yet available at this time.)

International Journal of Applied Earth Observation and Geoinformation 18 (2012) 407–416

Contents lists available at SciVerse ScienceDirect

International Journal of Applied Earth Observation and Geoinformation

journal homepage: www.elsevier.com/locate/jag

High-resolution satellite data reveal an increase in peak growing season gross primary production in a high-Arctic wet tundra ecosystem 1992–2008

Torbern Tagesson[a,*], Mikhail Mastepanov[a], Mikkel P. Tamstorf[b], Lars Eklundh[a], Per Schubert[a], Anna Ekberg[a], Charlotte Sigsgaard[c], Torben R. Christensen[a], Lena Ström[a]

[a] Department of Earth and Ecosystem Sciences, Lund University, Sölvegatan 12, 223 62 Lund, Sweden
[b] Department for Bioscience – Arctic Environment, Århus University, Frederiksborgvej 399, Roskilde DK-4000, Denmark
[c] Institute of Geography and Geology, University of Copenhagen, Øster Voldgade 10, DK-1350 Copenhagen, Denmark

ARTICLE INFO

Article history:
Received 18 July 2011
Accepted 27 March 2012

Keywords:
Light use efficiency
NDVI
Remote sensing
Climate change
FAPAR
GPP

ABSTRACT

Arctic ecosystems play a key role in the terrestrial carbon cycle. Our aim was to combine satellite-based normalized difference vegetation index (NDVI) with field measurements of CO_2 fluxes to investigate changes in gross primary production (GPP) for the peak growing seasons 1992–2008 in Rylekærene, a wet tundra ecosystem in the Zackenberg valley, north-eastern Greenland. A method to incorporate controls on GPP through satellite data is the light use efficiency (LUE) model, here expressed as $GPP = \varepsilon_{peak} \times PAR_{in} \times FAPAR_{green\_peak}$; where ε_{peak} was peak growing season light use efficiency of the vegetation, PAR_{in} was incoming photosynthetically active radiation, and $FAPAR_{green\_peak}$ was peak growing season fraction of PAR absorbed by the green vegetation. The ε_{peak} was measured for seven different high-Arctic plant communities in the field, and it was on average 1.63 g CO_2 MJ^{-1}. We found a significant linear relationship between $FAPAR_{green\_peak}$ measured in the field and satellite-based NDVI. The linear regression was applied to peak growing season NDVI 1992–2008 and derived $FAPAR_{green\_peak}$ was entered into the LUE-model. It was shown that when several empirical models are combined, propagation errors are introduced, which results in considerable model uncertainties. The LUE-model was evaluated against field-measured GPP and the model captured field-measured GPP well (RMSE was 192 mg CO_2 m^{-2} h^{-1}). The model showed an increase in peak growing season GPP of 42 mg CO_2 m^{-2} h^{-1} y^{-1} in Rylekærene 1992–2008. There was also a strong increase in air temperature (0.15 °C y^{-1}), indicating that the GPP trend may have been climate driven.

1. Introduction

Climate warming is proceeding faster in the Arctic than elsewhere on Earth, and current estimates suggest a substantial potential for change in these regions (ACIA, 2005). Terrestrial ecosystems of the Arctic currently store large amounts of carbon, and while the northern permafrost region covers only about 16% of the global soil area, it holds approximately 50% of the global below-ground organic carbon pool (McGuire et al., 2009; Tarnocai et al., 2009). Wet tundra ecosystems play a key role in controlling the terrestrial carbon cycle since the prevailing waterlogged, anoxic and cool soil conditions effectively reduce the rates of soil organic matter decomposition, which favors the formation of peat. Peat accumulation is primarily governed by the balance between carbon uptake by gross primary production (GPP) and carbon release through respiration. Changes in the sink strength of high-Arctic ecosystems are therefore highly affected by responses of these processes to climate variations. Several studies that investigated remotely sensed data from satellites and the normalized difference vegetation index (NDVI) have shown that there is a greening trend in northern ecosystems, indicating an increase in plant productivity (e.g. Myneni et al., 1997; Verbyla, 2008). These studies were mainly based on remote sensing data, and did not include in situ measurements. Additionally, they have mainly focused on boreal, low-Arctic, and sub-Arctic areas and very few studies exist from the high-Arctic. In the high-Arctic, temperatures are colder, and the growing season is shorter than in lower Arctic regions. Consequently, high-Arctic ecosystems normally experience greater temperature constraints, which presumably make them more sensitive to rising temperatures.

A widely applied approach within remote sensing is to estimate plant productivity by a light use efficiency (LUE) model (Monteith,

* Corresponding author. Tel.: +46 0704 993936; fax: +46 046 2220321.
E-mail addresses: torbern.tagesson@nateko.lu.se (T. Tagesson), mikhail.mastepanov@nateko.lu.se (M. Mastepanov), mpt@dmu.dk (M.P. Tamstorf), lars.eklundh@nateko.lu.se (L. Eklundh), per.schubert@nateko.lu.se (P. Schubert), anna.ekberg@nateko.lu.se (A. Ekberg), Cs@geo.ku.dk (C. Sigsgaard), torben.christensen@nateko.lu.se (T.R. Christensen), lena.strom@nateko.lu.se (L. Ström).

0303-2434/$ – see front matter © 2012 Elsevier B.V. All rights reserved.
http://dx.doi.org/10.1016/j.jag.2012.03.016

1972, 1977). The LUE-model allows GPP to be estimated from the photosynthetically active radiation absorbed by the green vegetation ($APAR_{green}$). $APAR_{green}$ can in turn be computed from incoming photosynthetically active radiation (PAR_{in}) and the fraction of photosynthetically active radiation absorbed by the green vegetation ($FAPAR_{green}$). This turns the LUE-model into:

$$GPP = \varepsilon \times PAR_{in} \times FAPAR_{green} \quad (1)$$

where ε is the light use efficiency of the vegetation. Here, GPP was defined as the total hourly ecosystem photosynthesis (g CO_2 m^{-2} h^{-1}). The LUE-coefficient (ε) was initially considered to be relatively constant, but substantial differences have been found between plant communities, development stage, species composition, and stress level (Goetz and Prince, 1996; Gower et al., 1999). It is therefore important to assess LUE for various plant communities when GPP is to be estimated over a larger area. Several studies including various vegetation types have shown a near-linear or linear correlation between FAPAR and NDVI (e.g. Huemmrich et al., 2010; Myneni and Williams, 1994). Consequently, satellite-based NDVI is commonly used to estimate FAPAR.

The main objective of the study was to investigate if there has been a change in peak-growing season GPP from 1992 to 2008 in Rylekærene, a high-Arctic wet tundra ecosystem. A second aim was to parameterize the LUE-model for the peak growing season for the plant communities dominating the area, and to investigate the relationship between in situ measured $FAPAR_{green}$ from the peak growing season and remotely sensed NDVI.

2. Materials and methods

2.1. Site description

The study took place in Rylekærene, a wet tundra ecosystem in the Zackenberg Research Area (74°28′N 20°34′W), in north-eastern Greenland. The Zackenberg valley is located in the high-Arctic zone but has a relatively mild climate due to its coastal location. Average temperature of the warmest month is 5.8 °C, and mean annual temperature is −9 °C (GeoBasis, 2010). The Zackenberg valley is underlain by continuous permafrost and the active layer thickness ranges between 0.5 and 1.0 m (GeoBasis, 2010). Since 1995, extensive ecological, biogeographic, climatic, and hydrological research and monitoring has been carried out in the Zackenberg research area (Meltofte et al., 2008).

To obtain a detailed description of the plant communities within the Rylekærene area, the dominant plant communities were recorded in the field every 15 m^2 within a 1.4 km^2 rectangle surrounding Rylekærene (Fig. 1). The 15 m^2 sampling plots were separated into the dominant plant communities identified in the area; continuous fen (flat areas dominated by *Eriophorum scheuchzeri*, *Carex stans* and *Dupontia psilosantha*), hummocky fen (hummocks dominated by *Eriophorum triste, Salix arctica* and *Arctagrostis latifolia*), grassland (dominated by *A. latifolia*, *E. triste*, and *Alopecurus alpinus)*, *S. arctica* snowbed, *Cassiope tetragona* heath, *Dryas octopetala* heath, and *Vaccinium uliginosum* heath. Non-vegetated areas were separated into gravel and water. This 1.4 km^2 rectangle will from now on be referred to as the study area.

2.2. Snow data, in situ NDVI and satellite-based NDVI

The start of the growing season carbon exchange is highly governed by day of year (DOY) of snowmelt in Arctic ecosystems (Mastepanov, 2010). The snow depth has been measured continuously since 1998 at the climate station (C1) in the center of the Zackenberg valley (Fig. 1) (GeoBasis, 2010). The floor of the Zackenberg valley is relatively flat, and it is assumed that the conditions at C1 are also representative for the study area. The DOY when snow depth decreased below 10 cm was used as a proxy for DOY of snowmelt end (DOY_{10cm}). Modeled snow cover from 1989 to 2004 (Buus-Hinkler et al., 2006) were used to estimate DOY_{10cm} before 1998. An ordinary least-squares linear regression was fitted between the DOY_{10cm} and modeled DOY with 18% snow cover of the Zackenberg valley for the years 1998–2004 ($R^2 = 0.96$, $p < 0.0001$, $df = 5$). Snow cover of 18% was used as a proxy for DOY of snow melt end since the major snow period is considered to end when the snow cover drops below this percentage (Buus-Hinkler et al., 2006). The regression line was then used to estimate DOY_{10cm} for 1992 to 1997.

In 2008 and 2009, incoming and reflected red (centered at 655 nm, bandwidth 48 nm) and near infrared (centered at 856 nm, bandwidth 56 nm) radiation was measured at the tower site (Fig. 1) using vertically oriented hemispherical two channel sensors (SKR 1800, Skye instruments, Llandridod wells, UK) during the periods 24 June to 1 September 2008, and 16 May to 26 August 2009. These data were used in a pre-analysis to determine the peak-period of NDVI during the growing season. The in situ measured radiation was used to estimate NDVI as:

$$NDVI = (\rho_{NIR} - \rho_{red})/(\rho_{NIR} + \rho_{red}) \quad (2)$$

where ρ_{NIR} and ρ_{red} are the hemispherical-directional reflectance factors in the near infrared (NIR) and the red bands, respectively. Based on the in situ measurements of NDVI in 2008 and 2009, the period between 35 and 51 days after DOY_{10cm} were empirically chosen to represent the peak season (Fig. 2). High-resolution satellite images acquired on cloud free days with high quality within this period of the growing seasons 1992–2008 were downloaded from EarthExplorer (2010) and included in the analysis (Table 1). Satellite data at this high-Arctic site are not stored on a regular basis. Furthermore, cloudy conditions decrease the number of available images. Therefore, we have chosen to combine data from different sensors in the analysis.

Radiance measured from satellites is affected by the atmosphere (aerosols, haze, cloud shadows, atmospheric depth and water vapor), illumination variations, and slope of the terrain (reflections from adjacent pixels and shadowing effects). To be able to compare images between dates and years, all satellite imagery was converted to reflectance and atmospheric and terrain corrections were performed with the software ATCOR 3. This method uses look-up tables derived with the Modtran® 4 radiative transfer code covering a wide range of weather conditions, sun angles, and ground elevations. In addition to the preprocessing of the satellite images, sixteen ~100 m^2 points of non-vegetated flat rock surfaces assumed not to vary in reflectance between years were used as reference points to enable comparison of satellite reflectance data between years. Linear regressions with intercept set to zero were fitted with reference reflectance of all the satellite images against reference reflectance 2007. The slope of the lines was used as correction factors to recalculate reflectance of all satellite images to be comparable with 2007 (ρ_{red}: R^2 range 0.32–0.95, average R^2 0.66; ρ_{NIR}: R^2 range 0.27–0.91, average R^2 0.55). The satellite sensors provide different spatial resolution and to match data when comparing satellite imagery with differently sized pixels all images were resampled to 1 m^2 using nearest-neighbor interpolation. The average reflectance for the corresponding 15 m vegetation cover plots was subsequently calculated for each image. Finally, the NDVI was estimated according to Eq. (2) for all satellite images. The relationship between FAPAR and NDVI is relatively insensitive to pixel heterogeneity, i.e., the combination of FAPAR and NDVI is insensitive to vegetation types and different configurations of ground cover and leaf area index (Myneni and Williams, 1994). This also results in a scale independent relationship in which the same NDVI is likely to correspond to the same FAPAR, irrespective of pixel

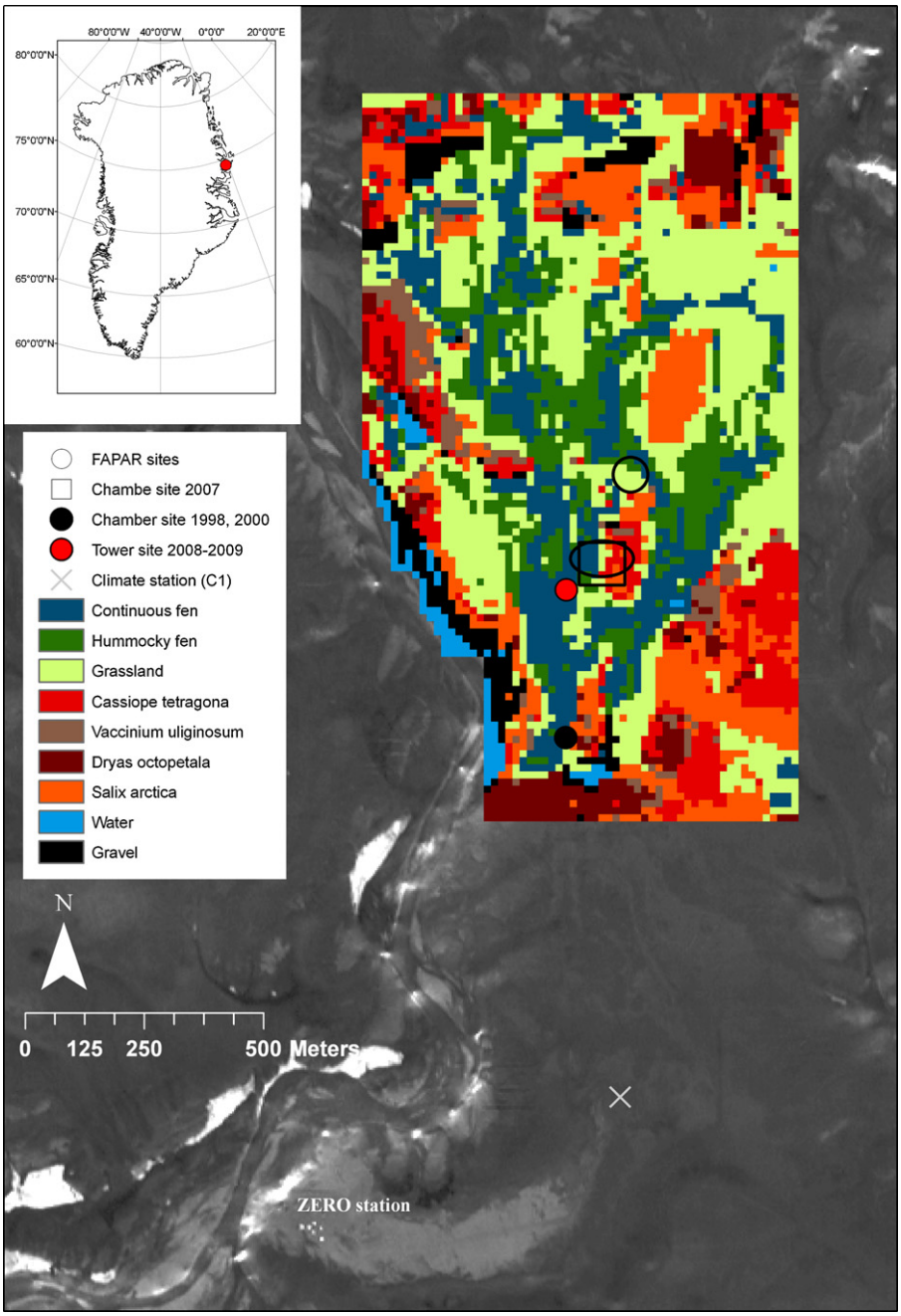

Fig. 1. The Zackenberg valley and the investigation area surrounding the research station (ZERO). The field-inventory map of the dominant plant communities observed in the Rylekærene study site is superimposed over an IKONOS satellite image from 23 July 2000 covering the Zackenberg valley. The red dot on the Greenland map is the location of Zackenberg. (For interpretation of the references to color in this figure legend, the reader is referred to the web version of the article.)

spatial scale (Myneni and Williams, 1994). This validates the use of NDVI in heterogeneous areas with different vegetation types and with different satellite sensor data.

2.3. Ground-based estimates of $FAPAR_{green}$ and its relationship to NDVI

The ASTER image from 2005 was used to select two sites within Rylekærene representing a wide range of NDVI for detailed ground-based $FAPAR_{green}$ plot measurements (Fig. 1). A total of 13 sampling plots were laid out at the two sites, covering all plant communities. The method from Schubert et al. (2010) was used to estimate $FAPAR_{green}$. Incoming PAR (PAR_{in}) and reflected PAR (PAR_{out}) were measured with hemispherical JYP-1000 sensors (SDEC Tauxigny, France) connected to Minicube loggers (EMS, Brno, Czech Republic). The measurement interval was thirty seconds and data were averaged over 10 min periods between 25 June and 5 August 2007. The fraction of absorbed photosynthetically active radiation by the total ground surface ($FAPAR_{total}$) was calculated by:

$$FAPAR_{total} = \frac{PAR_{in} - PAR_{out}}{PAR_{in}} \quad (3)$$

Data acquired at solar elevation angles lower than 30° were removed to decrease the impact of low illumination angles.

We estimated the fraction of ground covered by photosynthetically active vegetation ($FRAC_{green}$) from vertical ground photographs taken the 2 and 4 August 2007 of a 0.50 m × 0.50 m sample plot under each sensor. Each sample plot was divided

Table 1
Summary of satellite image data for the different years. DOY_{10cm} is the day of year with 10 cm snow depth.

Date (M/D/Y)	Satellite sensor	ρ_{red} (range (μm))	ρ_{NIR} (range (μm))	DOY_{10cm}
8/7/1992	SPOT-2 HRV2	X2 (0.61–0.68)	X3 (0.78–0.89)	175
7/27/1995	Landsat 5 TM	TM3 (0.63–0.69)	TM4 (0.76–0.90)	164
7/31/1998	Landsat 5 TM	TM3 (0.63–0.69)	TM4 (0.76–0.90)	176
7/23/2000	IKONOS	B3 (0.63–0.70)	B4 (0.76–0.85)	165
7/31/2001	SPOT-4 HRV2	X2 (0.61–0.68)	X3 (0.78–0.89)	175
8/2/2002	Landsat 7 ETM+	ETM3 (0.63–0.69)	TM4 (0.76–0.90)	171
7/29/2004	Landsat 7 ETM+[a]	ETM3 (0.63–0.69)	TM4 (0.76–0.90)	164
7/25/2005	ASTER	B2 (0.63–0.69)	B3 (0.76–0.86)	158
7/29/2007	Landsat 7 ETM+[a]	ETM3 (0.63–0.69)	TM4 (0.76–0.90)	159
8/9/2008	Landsat 7 ETM+[a]	ETM3 (0.63–0.69)	TM4 (0.76–0.90)	175

[a] Images taken when the Scan Line Corrector on Landsat 7 was broken.

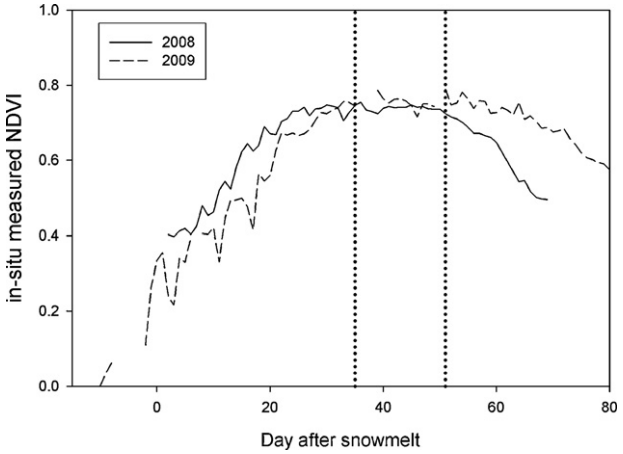

Fig. 2. The normalized difference vegetation index (NDVI) measured in situ during the growing seasons 2008 and 2009 at the tower site in Fig. 1. The dotted lines are the time window chosen to represent the peak growing season; days 35–51 after day of 10 cm snow depth.

into 25 0.10 m × 0.10 m sub-plots and the $FRAC_{green}$ was recorded. The photographs were taken 55–57 days after DOY_{10cm}. No photographs were available from 35 to 51 days after DOY_{10cm}. However, the vegetation had not yet started to senesce, and the photographs could thus still be used for estimation of $FRAC_{green}$. The $FRAC_{green}$ was, subsequently, multiplied by $FAPAR_{total}$ averaged from 13 to 29 July 2007 to compute $FAPAR_{green}$ for the same period

$$FAPAR_{green} = FAPAR_{total} \times FRAC_{green} \quad (4)$$

Since this estimate represents the peak growing season it will from now on be referred to as ground-based $FAPAR_{green\_peak}$. As previously mentioned it has been shown that FAPAR is linearly related to NDVI. We used a major-axis linear regression to estimate the relationship between the ground-based $FAPAR_{green\_peak}$ and NDVI based on a Landsat Enhanced Thematic Mapper (ETM+) image from 29 July 2007, in order to account for errors in both *x* and *y*.

2.4. Field measurements of CO_2 fluxes 30 June to 4 August 2007

A study site in the center of the Rylekærene was chosen to ensure that the main vegetation types were represented within a reasonably small area (Fig. 1). A total of 55 measurement plots were randomly distributed within the different plant communities; 15 plots in continuous fen, 10 plots each in hummocky fen and grassland, and 5 plots each in *S. arctica* snowbed, *C. tetragona* heath, *D. octopetala* heath, and *V. uliginosum* heath. CO_2 fluxes were measured using the closed chamber technique with an infrared gas analyzer (EGM-4, PP-systems, Hitchin, Hertfordshire, UK). The chamber was a transparent Plexiglas cube which covered 0.34 m^2 of ground and was 0.3 m high. The inlet and outlet of gas was located at one of the sides 0.25 m and 0.15 m above ground, respectively. To ensure proper mixing of the air and representative sampling from the entire chamber, two small fans were located in the upper part of the chamber. At each plot, net ecosystem exchange (NEE) was measured by placing the transparent Plexiglas chamber on the ground. The concentration of CO_2 inside the chamber was recorded continuously at 0.63 Hz for 3 min. The chamber was ventilated for 1.5 min between measurements. Ecosystem dark respiration (ER) was measured after the NEE measurement by covering the chamber with a lightproof hood. No bases inserted to the ground were used during the measurements. A linear regression was fitted to the concentration change in the chamber over the measurement period (Mastepanov, 2010). Measurements were distributed between 10 a.m. and 6 p.m. and were carried out 11 times at each of the 55 individual plots between 30 June and 4 August 2007. Gross primary production was calculated by subtracting ER from NEE, giving negative values to GPP in this first calculation step. Subsequently, we converted GPP to positive values defining ecosystem uptake of CO_2 (GPP) as positive and loss of CO_2 (ER) as negative. The CO_2 flux measurements were used for estimating average daytime CO_2 fluxes for the different plant communities. It could be seen in the CO_2 concentration data that 13 NEE measurements and 21 ER measurements were disturbed and these were removed from the rest of the analysis.

In addition, soil temperature at 10 cm depth, water table depth (for the fen communities), and active layer thickness were measured in close proximity to each plot during the chamber measurements.

2.5. Estimation of peak growing season light use efficiency

During each chamber measurement, PAR_{in} and PAR_{out} was measured at 0.77 Hz within the chamber with vertically mounted hemispherical JYP-1000 sensors. Subsequently, average values were calculated for the same periods as the CO_2 flux measurements. The PAR measurements were used for estimating $FAPAR_{total}$ inside the chamber (Eq. (3)). At each of the 55 chamber measurement plots, photographs were taken on the 2 and 4 August 2007 of a 0.50 m × 0.50 m square placed on the ground. Each plot was divided into 25 0.10 m × 0.10 m sub-plots and the $FRAC_{green}$ was recorded, whereupon Eq. (4) was used for estimating $FAPAR_{green}$. $FAPAR_{green}$ varies throughout the growing season (e.g. Gower et al., 1999), and all 11 measurement occasions could thus not be used for estimating $FAPAR_{green\_peak}$. We only used the measurements between 13 and 29 July (days 35–51 after DOY_{10cm}). This will from now on be referred to as chamber-based $FAPAR_{green\_peak}$ to separate it from ground-based $FAPAR_{green\_peak}$ measured at the 13 plots with different NDVI (see Section 2.3). As GPP, PAR_{in} and chamber-based $FAPAR_{green\_peak}$ were measured inside the chamber, they were all affected by the transparency of the chamber, and could thus be

related. These measurements were used to calculate the peak growing season ε (ε_{peak}) for each plot and each measurement between 13 and 29 July using the equation:

$$\varepsilon_{peak} = \frac{GPP}{PAR_{in} \times FAPAR_{green\_peak}} \quad (5)$$

Average ε_{peak} was estimated for each plant community and a one-way ANOVA Tukey's post hoc test assuming equal variances between groups was used to test for significant differences between the ε_{peak} of the different plant communities.

2.6. Evaluation of the LUE-model

In the LUE-modeling of peak growing season GPP, average ε_{peak} for each plant community (Section 2.5) was used together with the ground-based $FAPAR_{green\_peak}$ versus NDVI linear regression:

$$GPP = \varepsilon_{peak} \times PAR_{in} \times (k \times NDVI + m) \quad (6)$$

where k and m are model parameters from the ground-based $FAPAR_{green\_peak}$ versus NDVI linear regression (Section 2.3).

The same ground-based GPP measurements used for parameterization of the LUE-model were used in the evaluation of the modeled GPP 2007. Additionally, the closed chamber technique was used to perform ground-based measurements of GPP at six wet continuous fen plots during the summers 1998 and 2000 (Joabsson and Christensen, 2001). The measurements between 35 and 51 days after DOY_{10cm} from these datasets were used in the evaluation of LUE-modeled GPP. Additionally, Tagesson et al. (2012) measured NEE using the eddy-covariance technique during the field season 2008. NEE was partitioned into GPP and ER using light response curves:

$$GPP = -(F_{csat} + R_d) \times \exp^{((\alpha \times PAR_{in}/F_{csat} + R_d))} \quad (7)$$

where F_{csat} is CO_2 uptake at light saturation, R_d is dark respiration and α is the initial slope of the light response curve. We entered 1106 $\mu mol\,m^{-2}\,s^{-1}$ as incoming PAR to Eq. (7) (as we used 1106 $\mu mol\,m^{-2}\,s^{-1}$ as incoming PAR in the LUE-modeling of GPP 1992–2008 (see Section 2.7)) together with the parameters in the light response curve estimated by Tagesson et al. (2012) for the period of the satellite Image 2008 ($R^2 = 0.75$, $df = 191$).

In the LUE-modeling of GPP, the NDVI and PAR_{in} were used as input data in Eq. (6). The NDVI at the measurement plots were calculated from the satellite data in Table 1 (Eq. (2)). Incoming PAR measured inside the chamber was used in the model evaluation, since both PAR_{in} and GPP was reduced by the chamber. For 2008, the relative contribution of the different parts of the tower footprint from noon of the day of the satellite image was multiplied by the NDVI Image 2008 to estimate NDVI for the measured area. The ε_{peak} measured for the different plant communities was applied to the different plant communities in Fig. 1. The relative contribution of the footprint was multiplied by the ε_{peak} map, and an average ε_{peak} was hereby estimated for the measured area. The estimated average NDVI and average ε_{peak} was used in Eq. (6) together with PAR_{in} (1106 $\mu mol\,m^{-2}\,s^{-1}$), to LUE-model GPP at noon of the day of the satellite Image 2008.

Average field-measured GPP for each measurement plot was calculated with the measurements from between 35 and 51 days after DOY_{10cm}. This was done for the datasets from 1998, 2000, 2007 and 2008. The same procedure was used with the LUE-modeled GPP; an average for each measurement plot was calculated with the modeled values from between 35 and 51 days after DOY_{10cm}. An ordinary least-squares linear regression was fitted between the measurement plot averaged LUE-modeled and field-measured GPP. The mean difference between the LUE-modeled GPP and the field-measured GPP was estimated by computing a root mean square error (RMSE).

2.7. The spatial and temporal extrapolation of GPP 1992–2008

Incoming solar radiation has been measured hourly between 1996 and 2008 at the climate station C1 (Fig. 1) (GeoBasis, 2010). There was no trend in PAR_{in} 1996–2008 (GeoBasis, 2010), and we did not want to introduce errors due to weather conditions on the day of the satellite images. We therefore used average PAR_{in} at noon for the day of the satellite Images 1998–2008 (1106 ± 37 $\mu mol\,m^{-2}\,s^{-1}$) as PAR_{in} in Eq. (6) to model GPP for all years. Furthermore, the same irradiance was assumed over the entire study area since the satellite images were recorded on days with clear skies, and the study area was relatively small (1.4 km^2).

A Monte–Carlo sampling approach was adopted by sampling 2000 sets of model parameters. The model parameters were slope (k) and intercept (m) of the ground-based $FAPAR_{green\_peak}$ versus NDVI linear regression, and the measured ε_{peak} for the different plant communities (Eq. (6)). Water and gravel areas were assigned an ε_{peak} of zero. Average and standard deviation of the parameters in the $FAPAR_{green\_peak}$ versus NDVI linear regression were calculated in the regression analysis, and the average and standard deviation of the ε_{peak} was calculated from the field measurements. Each parameter was sampled randomly 2000 times in a normal distribution around the average. The 2000 sets of ε_{peak} for the different plant communities were applied to the plant communities in Fig. 1. To model noon-time GPP for Rylekærene these 2000 sets of ε_{peak} and parameters of the $FAPAR_{green\_peak}$ versus NDVI linear regression were put into Eq. (6). These 2000 sets of Eq. (6) were finally applied to the average PAR_{in} and to each of the NDVI datasets for the study area derived from the 1992 to 2008 satellite images in Table 1. Average values and standard deviations of the 2000 model runs were estimated for each year, where standard deviation gives the model uncertainty. The variation in GPP due to heterogeneity in the study area was not included in the model uncertainty as average values of the study area were first calculated. Standard deviation was strictly an estimate of the uncertainty in the LUE-modeled GPP. Plant community composition was set to be static between 1992 and 2008.

Between 1996 and 2008 air temperature was measured at C1 (Fig. 1), and annual averages were calculated for each individual year (GeoBasis, 2010). Air temperature data at C1 from 1992 to 1996 was obtained from a linear relationship ($R^2 = 0.86$, $n = 12$) against air temperature at Danmarkshavn (Cappelen, 2007). Using the growing season temperature would be more appropriate, however, no small-scale temporal dataset of temperature existed before 1996, and we therefore chose to show annual averages instead. However, summer temperatures were following the same trend as the annual averages 1996–2008 (GeoBasis, 2010).

Sen's method with the nonparametric Mann–Kendall's test was used for estimating the slope and the significance of the linear trend in NDVI, LUE-modeled GPP and annual air temperature 1992–2008.

3. Results

3.1. Ground-based $FAPAR_{green\_peak}$ and satellite-based NDVI

There was a significant linear relationship between ground-based $FAPAR_{green\_peak}$ and NDVI ($R^2 = 0.60$, $p = 0.002$, $df = 12$) (Fig. 3). NDVI calculated from the 29 July 2007 satellite image was on average 0.56 with a standard deviation of 0.07, in the plots where ground-based $FAPAR_{green\_peak}$ was measured, and ground-based $FAPAR_{green\_peak}$ in the respective plots were on average 0.59 with a standard deviation of 0.09.

Table 2
Average measured CO_2 fluxes and abiotic parameters for the different plant communities measured between 10 a.m. and 6 p.m. the 30 June to 4 August 2007 (±1 standard deviation). NEE is the net ecosystem exchange, ER is the ecosystem respiration, and GPP is the gross primary production. "–" means that no measurements were performed. Active layer is the average from the 4 August 2007 when the thickest active layer was measured.

Plant communities	Soil temp 10 cm (°C)	Active layer (cm)	Water table depth (cm)	NEE ($mg\,CO_2\,m^{-2}\,h^{-1}$)	ER ($mg\,CO_2\,m^{-2}\,h^{-1}$)	GPP ($mg\,CO_2\,m^{-2}\,h^{-1}$)	Sample size
Continuous fen	7.4 ± 1.3	49 ± 3	−3.4 ± 3.6	289.5 ± 164.4	−369.2 ± 148.0	654.1 ± 250.1	154
Hummocky fen	7.4 ± 1.3	47 ± 4	−8.2 ± 4.2	252.4 ± 225.7	−350.1 ± 138.5	581.1 ± 281.4	108
Grassland	6.0 ± 1.3	56 ± 8	–	144.1 ± 113.8	−332.1 ± 132.6	475.1 ± 190.0	110
Salix arctica snowbed	8.2 ± 2.1	78 ± 3	–	36.9 ± 103.5	−207.6 ± 121.1	239.2 ± 127.6	51
Vaccinium uliginosum Heath	7.6 ± 2.3	69 ± 5	–	30.5 ± 67.2	−187.4 ± 89.4	217.6 ± 117.5	54
Cassiope tetragona heath	7.7 ± 1.6	74 ± 6	–	22.8 ± 76.7	−187.5 ± 92.4	215.0 ± 103.6	54
Dryas octopetala heath	8.9 ± 2.1	75 ± 5	–	38.2 ± 84.0	−139.6 ± 80.2	188.2 ± 94.7	54

3.2. CO_2 fluxes and environmental variables measured between 10 a.m. and 6 p.m. 30 June to 4 August 2007

Average GPP ranged from 188.2 to 654.1 $mg\,CO_2\,m^2\,h^{-1}$ for the different plant communities, where continuous fen had the highest GPP and *D. octopetala* heath had the lowest. Average ecosystem respiration (ER) ranged from −139.6 to −369.2 $mg\,CO_2\,m^2\,h^{-1}$, again with *D. octopetala* heath with lowest absolute values of respiration, and continuous fen with the highest. Combined, this gave a NEE ranging from 22.8 $mg\,CO_2\,m^2\,h^{-1}$ to 289.5 $mg\,CO_2\,m^2\,h^{-1}$, where continuous fen had the highest CO_2 uptake and *C. tetragona* heath had the lowest (Table 2).

Water table depths were on average 3.4 cm below the ground surface for continuous fen and 8.2 cm below the surface for hummocky fen (it was not measured in grassland, *S. arctica* snowbed, *C. tetragona* heath, *D. octopetala* heath, and *V. uliginosum* heath, since these plots were too dry to find a water table). The average peak active layer thickness ranged from 47 cm to 78 cm, for the different plant communities. Elevated/drier plant communities had a thicker active layer than the wetter plant communities (Table 2).

3.3. Chamber-based $FAPAR_{green\_peak}$ and ε_{peak}

The average chamber-based $FAPAR_{green\_peak}$ was 0.60 and ranged between 0.36 and 0.77 for the different plant communities, with the highest values for fen communities and the lower for drier heath communities (Table 3). The peak light use efficiency (ε_{peak}) varied between 0.70 $g\,CO_2\,MJ^{-1}$ and 2.45 $g\,CO_2\,MJ^{-1}$, with an average of 1.63 $g\,CO_2\,MJ^{-1}$ (Table 3). According to the one-way ANOVA Tukey's post hoc test, there were significant differences in ε_{peak} between all plant communities, except for between *S. arctica* snowbed and *V. uliginosum* heath.

Table 3
The peak growing season light use efficiency (ε_{peak}) and the average chamber-based fraction of photosynthetically active radiation absorbed by the green vegetation ($FAPAR_{green\_peak}$) for the different plant communities. Average values ±1 standard deviation.

Plant communities	$FAPAR_{green\_peak}$	ε_{peak} ($g\,CO_2\,MJ^{-1}$)	Sample size
Continuous fen	0.72 ± 0.05	2.45 ± 1.13	52
Hummocky fen	0.77 ± 0.05	2.20 ± 1.28	39
Grassland	0.65 ± 0.10	1.98 ± 1.22	42
Salix arctica snowbed	0.40 ± 0.10	1.38 ± 0.83	15
Vaccinium uliginosum heath	0.36 ± 0.17	1.30 ± 0.70	19
Cassiope tetragona heath	0.43 ± 0.05	0.70 ± 0.36	20
Dryas octopetala heath	0.36 ± 0.06	0.83 ± 0.49	16
Total	0.60 ± 0.06	1.63 ± 0.92	176

3.4. Evaluation of the LUE-model

There was a significant linear relationship between GPP modeled with Eq. (6) and the ground-based field measurements of GPP (slope 0.66; intercept 179.2, $R^2 = 0.58$, $n = 68$) (Fig. 4). On average (±1 standard deviation) the LUE-modeled GPP ($520 \pm 253\,mg\,CO_2\,m^{-2}\,h^{-1}$) was very similar to the field-measured GPP ($520 \pm 294\,mg\,CO_2\,m^{-2}\,h^{-1}$). The RMSE was 192 $mg\,CO_2\,m^{-2}\,h^{-1}$. The GPP model performed well in 2000, 2007, and 2008 with fractions of LUE-modeled GPP against

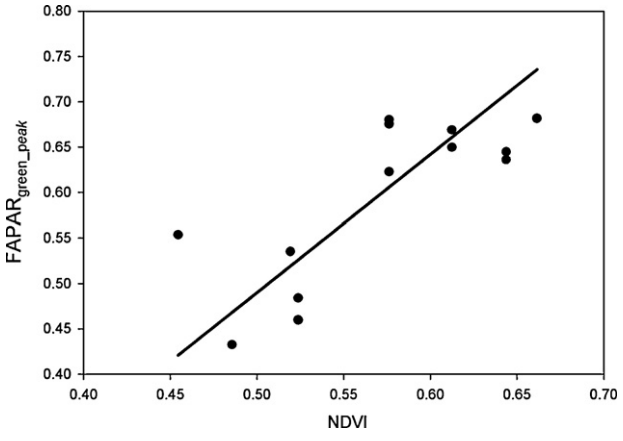

Fig. 3. The ground-based fraction of photosynthetically active radiation absorbed by the green vegetation during the peak growing season ($FAPAR_{green\_peak}$) against satellite-based normalized difference vegetation index (NDVI) from Landsat ETM7+ 29 July 2007. The fitted regression line is $FAPAR_{green\_peak} = 1.52 \times NDVI - 0.27$, ($R^2 = 0.60$, $p = 0.002$, $df = 12$).

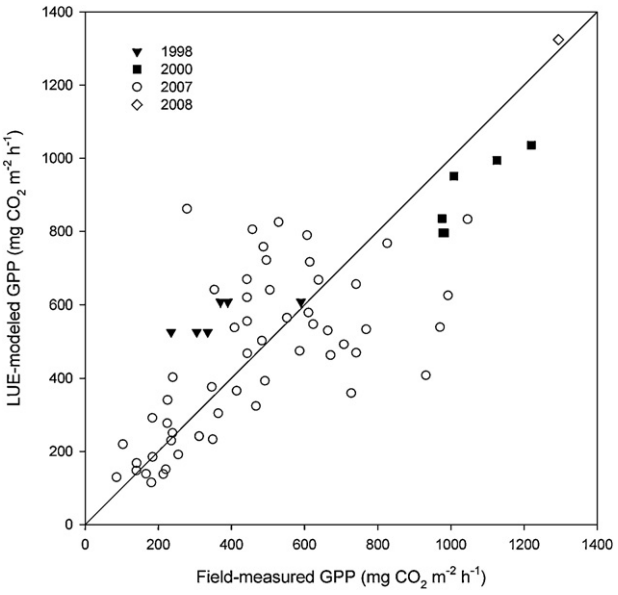

Fig. 4. Evaluation of the light use efficiency modeled gross primary production (LUE-modeled GPP) modeled with Eq. (6) against field-measured GPP, which were made in 1998, 2000, 2007 and 2008. The line represents the 1:1 relationship.

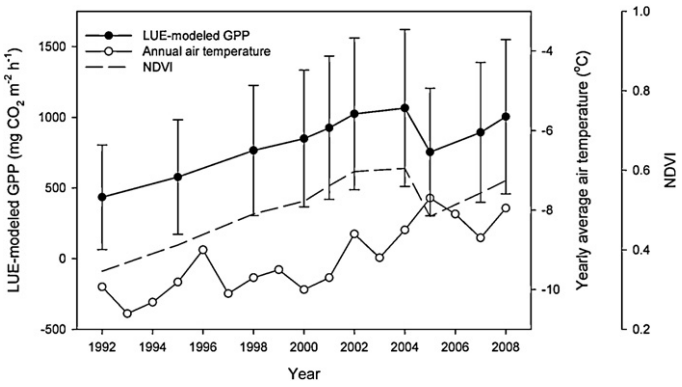

Fig. 5. The light use efficiency modeled gross primary production (LUE-modeled GPP) modeled with Eq. (6), average annual air temperature and satellite-based normalized difference vegetation index (NDVI) 1992–2008. Gross primary production is an average of 2000 Monte–Carlo sampled simulations, and the error bars are one standard deviation of the 2000 model runs.

field-measured GPP of 0.86, 0.99, and 1.02, respectively. For 1998, the fraction was 1.53.

3.5. Temporal trends in LUE-modeled GPP between 1992 and 2008

There was a strong overall increase in NDVI from 1992 to 2008 (Sen's slope: 0.014 y^{-1}, significant according a 95% confidence interval), indicating a greening trend in Rylekærene (Fig. 5). Sen's slope (significant according a 95% confidence interval) indicated that the average annual increase in LUE-modeled GPP between 1992 and 2008 corresponded to 42 mg CO_2 m^{-2} h^{-1} y^{-1} (Fig. 5). The increase was especially clear between 1992 and 2002, whereafter the increase slowed down (Fig. 5). In 2005 there was a drop in LUE-modeled GPP. This was followed by an increase in LUE-modeled GPP, and in 2008 the GPP was back at the 2000 level (Fig. 5). There was a high standard deviation for LUE-modeled GPP throughout the time interval, on average ±481 mg CO_2 m^{-2} h^{-1} (Fig. 5), indicating considerable model uncertainty. Sen's slope (significant according a 99% confidence interval) showed that the average annual air temperature increase 1992–2008 was 0.15 °C y^{-1} (Fig. 5).

4. Discussion

4.1. Temporal trends in LUE-modeled GPP 1992–2008

The overall increase in LUE-modeled GPP between 1992 and 2008 (Fig. 5) is in agreement with expectations for high-latitude ecosystems as the climate is warming (e.g. Oechel et al., 2000). Correspondingly, we found that the average annual air temperature in or in close proximity to the Zackenberg area also increased between 1992 and 2008 (Fig. 5). This observation is supported by a range of other studies. Wania et al. (2009) modeled strong increases in Arctic annual NPP until 2000 using a dynamic global vegetation model (DGVM). The NPP trend was caused by a strong sensitivity to changes in air temperature. Grøndahl et al. (2008) measured NEE 1997–2005 at a heath site in the vicinity of the climate station (C1) in the Zackenberg valley. There was an increase in absolute values of growing season cumulative NEE 1997–2005, and they were strongly correlated to air temperature (Grøndahl et al., 2008). Parmentier et al. (2011) showed a strong correlation between interannual variation in GPP estimated from eddy covariance measurements in north-eastern Siberia and air temperature. However, there was no trend in GPP 2003–2010.

The observed increase in NDVI is consistent with other studies investigating NDVI trends in the Arcic (Jia et al., 2003; Myneni et al., 1997; Slayback et al., 2003; Stow et al., 2007; Verbyla, 2008; Zhou et al., 2001). However, these studies showed lower increases in NDVI (~0.003–0.006 y^{-1}) than in the study area. These trends were based on relatively coarse spatial scales (pixel size ≥ 1 km^2), and a 1 km^2 sample plot include a large fraction of gravel, rock and water in the Arctic. These areas have relatively constant NDVI over time and a large fraction of the satellite pixel is hereby not affected by the general NDVI trend. The 1.4 km^2 study area is almost completely covered by plant communities (Fig. 1), and the entire study area contributes to the observed change in NDVI, which could possibly result in an apparent larger increase than for the other studies.

The temperature increased gradually 1992–2008, whereas there was an increase in modeled GPP until 2004. After 2004 there was a decline which then was followed by a recovery (Fig. 5). An explanation to the weakened response to an increased temperature may be that the species dominating the Zackenberg area have arrived from north of the inland ice, and are consequently adapted to lower temperatures (Bay, 1992). It could be that the plants have reached their immediate capabilities of growth and a further increase in temperature does not enhance their GPP (Callaghan et al., 2005). There could also be species interactions. Increased growth of one species could decrease the growth of another, which would give negligible change in the community growth (Callaghan et al., 2005). A further explanation could be that the nutrient mineralization rates stimulated by the increased temperatures are not sustained in the long run which leads to nutrient limitation (Callaghan et al., 2005).

4.2. The 2005 decrease in LUE-modeled GPP

The LUE-modeled GPP showed a clear drop in 2005 (Fig. 5). This year had the earliest snowmelt (DOY_{10cm} 158) and the highest average annual temperature. It was the third year in a row with low precipitation (GeoBasis, 2010), hence water limitation might explain the decrease in LUE-modeled GPP. Additionally, the temperature was unusually high during winter and spring of 2005 which leads to several thaw events and an unusually low snow-cover (GeoBasis, 2010). It has been shown that winter warming episodes can lead to extensive vegetation damage and reduction in plant productivity over large areas (Bokhorst et al., 2009). However, contrary to our observations, there was no apparent decrease in the measured NEE in 2005 at the heath site in the vicinity of the climate station (C1) (Grøndahl et al., 2008) Additionally, according to a single grid cell subset of the peak growing season 8-day GPP (Collection 5.1) composites extracted for 2000–2008 from the MODIS/Terra L4 1000 m collection (MOD17A2_51) from the center of the Rylekærene (ORNL DAAC, 2012), there was no decrease in peak growing season GPP in 2005. The inter-annual variation in peak growing season LUE-modeled GPP 2000–2008 was well explained by the inter-annual variation in the peak growing season MODIS GPP product for all years but 2005. This indicates that neither water limitation nor vegetation damages can explain the LUE-modeled GPP decrease in 2005.

In the reference reflectance analysis against the 2007 image (Section 2.2), the ASTER image from 2005 was the image with the worst fit (R^2 ρ_{red}: 0.32 and ρ_{NIR}: 0.27). Although the satellite imagery were preprocessed, there may still be some errors in the remotely sensed data related to cloudiness, reflectance from the atmosphere, adjacency effects, geometry of the sun and the sensor, sensor degradation and topography. Another plausible explanation is that ASTER usually produce lower NDVI values than Landsat ETM+ (Xu and Zhang, 2010). The reason is that the relative spectral response of the ASTER sensor enters the red edge area, whereas the

Landsat ETM+, never touches it (Xu and Zhang, 2010). This should not be an issue for the IKONOS (Cook et al., 2001) or the Landsat TM (Chander et al., 2009) images. SPOT generally creates a NDVI that is ~4% larger than Landsat TM5, due to the relative spectral response of the ρ_{NIR} band (Franke et al., 2006). In this analysis, SPOT images were used for 1992 and 2001. Lowering the NDVI values by 4% for these years would not have any significant effect on the analysis. Hence, the general conclusion is that the decrease in LUE-modeled GPP 2005 was caused by an erroneous estimate from the ASTER image, and not a real decrease caused by vegetation damage or water limitation.

4.3. The relationship between ground-based $FAPAR_{green\_peak}$ and NDVI and the ε_{peak} of high-Arctic vegetation

In accordance with several previous studies (e.g. Huemmrich et al., 2010; Myneni and Williams, 1994), we found a significant linear relationship between NDVI and ground-based $FAPAR_{green\_peak}$ for the high-Arctic wet tundra ecosystem in Rylekærene. The major sources of error are the scale-dependent generalization of measured ground-based $FAPAR_{green\_peak}$ and errors in the remotely sensed data. Ground-based $FAPAR_{green\_peak}$ was measured at a plot-scale and assumed to be similar over the entire NDVI pixel. In the field there are small scale differences within the pixel due to micro-topography, soil type, and vegetation structure and distribution. However, the significant linear relationship between ground-based $FAPAR_{green\_peak}$ and NDVI indicate that the measured areas under the FAPAR sensors were reasonably representative for the entire NDVI pixels.

In a worldwide comparison, ε_{peak} in Rylekærene was low ($1.63\,g\,CO_2\,MJ^{-1}$). If it is assumed that 50% of GPP goes to net primary production (NPP) (Schlesinger, 1997), this would result in an average ε_{peak} for NPP of $0.22\,g\,C\,MJ^{-1}$ in Rylekærene. This is almost half of the modeled worldwide average ε of $0.43\,g\,C\,MJ^{-1}$ (Ruimy et al., 1999). However, Arctic ecosystems are constrained in their productivity due to extreme temperatures, short growing seasons, low water and nutrient availability and, low quantum input. The observed ε_{peak} was similar to values found for plant communities of the Alaskan north slopes (Huemmrich et al., 2010). They were, however, quite large in comparison to the ε_{peak} ($\sim 0.1\,g\,C\,MJ^{-1}$) for Arctic tundra estimated by process-based modeling (Ito and Oikawa, 2004).

Errors in the estimates of the ε_{peak} mainly derive from the field measurements of GPP and APAR. There are potential errors with the closed chamber technique used for estimating GPP of the different plant communities (Davidson et al., 2002; Mastepanov, 2010). No control of either temperature or pressure inside the chamber headspace was applied in this study. However, the chamber was not completely air tight, and as the gas concentration increased very linearly, pressure anomalies and temperature alterations should be minimal. The measured CO_2 fluxes (Table 2) were in the same range as other studies in Arctic ecosystems, using both eddy covariance and closed chamber techniques (Arndal et al., 2009; La Puma et al., 2007; Lafleur and Humphreys, 2007; Nobrega and Grogan, 2008; Soegaard and Nordstroem, 1999). There can, further, be errors in the chamber-based $FAPAR_{green\_peak}$ measurements. The PAR sensors measured hemispherically and the results may be somewhat affected by the chamber walls. However, the chamber-based $FAPAR_{green\_peak}$ was on average 0.60, which is almost exactly the same as the ground-based $FAPAR_{green\_peak}$ (0.59), measured without chamber in the same area.

4.4. Model uncertainty

In the GPP model (Eq. (6)) we combined the linear regression between ground-based $FAPAR_{green\_peak}$ and NDVI with ε_{peak}. These input variables were based on field measurements, which naturally often have a high variation in both the spatial and temporal domain. By this approach we built the variation in field data into the GPP model and created uncertainties, which propagated during the modeling process. This explains the large model standard deviation seen in Fig. 5. Furthermore, the linear regression between the LUE-modeled GPP and field-measured GPP indicates that the GPP model did not fully capture all variance seen in the field data. The LUE-modeled GPP is based on average values in the parameters and the input data, whereas there is a large natural variation in the field-measured GPP. The ε_{peak} for the different plant communities had large variation as seen in the standard deviation in Table 3. Additionally, the NDVI data were based on 4–30 m sized pixels (depending on satellite sensor), and the satellite data were thus average values of the spatial heterogeneity in the pixels.

The GPP model performed well in 2007 and 2008. In these years the model evaluation was based on data with a relatively large area covered. In 1998 and 2000, the measurement plots in the model evaluation were clumped to one site. The years 1998 and 2000 were thus more vulnerable to the small-scale spatial heterogeneity of the area. This large natural variation in the spatial domain can also be seen in the large scatter of the 2007 evaluation data in Fig. 4. The year 1998 had the weakest model performance, and it was also the year where the evaluation was based on only two satellite pixels.

The LUE-model represents a generalized picture of all processes affecting GPP. There are other approaches in modeling GPP, such as, the light response curve (Eq. (7)) (e.g. Falge et al., 2001; Tagesson and Lindroth, 2007), the radiation, temperature and CO_2 concentration dependent nonrectangular hyperbola model (Cannell and Thornley, 1998), or more advanced biochemical models (Farquhar et al., 1980). The advantage with the more advanced models is that the underlying mechanisms in the system can be analyzed. Still, the LUE-model is a robust approximation and has been shown to work well in tundra regions, both on widespread temporal and spatial scales (Huemmrich et al., 2010; Shaver et al., 2007; Street et al., 2007). The appeal with the LUE-model is its dependence on a limited number of variables. This is an important advantage when dealing with the problem of error propagation.

The ε_{peak} was derived from 55 measurement plots measured between 13 and 29 July 2007. A potential source of error may be that this mainly spatially varying ε_{peak} was applied in the temporal domain 1992–2008. The ε_{peak} is changing over the season and with changing environmental conditions. We hope to have circumvented these problems by choosing to apply the model strictly to a peak growing season time window for the satellite images. In accordance, there was no sensitivity of the modeled GPP to the DOY and day after DOY_{10cm} for the satellite images. A drawback with only applying the model to the peak growing season was that the annual integrals of GPP could not be estimated, which would have provided further understanding in the trends in carbon dynamics during the study period 1992–2008. The annual integral of GPP is not only affected by the GPP maxima, but also the length and the shape of the growing season.

The ε in the LUE-model is affected by the temperature and could thus change over the years. However, in a nonrectangular hyperbola model by Cannell and Thornley (1998), ε was set to a constant below 15 °C, which is well above most growing season temperatures in Rylekærene. It was also shown that neither warming nor changes in the water table depth altered the GPP versus APAR relationship for the ecosystems of the Alaskan north slopes (Huemmrich et al., 2010). Additionally, changes in seasonal length and warming did not alter the photosynthetic capacity of seven tundra plant species (Starr et al., 2008). The ε is also affected by the air CO_2 concentration. However, the 29 ppm change in CO_2 concentration in the atmosphere from 1992 to 2008 (Tans, 2009) should

not have altered ε more than 3%, according to the relationship in Cannell and Thornley (1998).

An additional source of error is possible changes in the vegetation types, as have been reported to occurred in low-Arctic and sub-Arctic areas (ACIA, 2005). The spatial coverage of the plant communities is set to be static since we only had estimates from 2007 (Fig. 1). However, in the area surrounding the chamber measurement site 1998–2000 (Fig. 1) it has been noted that the *A. latifolia* has become more abundant between 2000 and 2008. This indicates drier conditions at this site. The plant community composition was estimated in 1997 in a ~12% part of the study area (Christensen et al., 2000). In a comparison between Fig. 1 from 2007 and the plant community composition from 1997, the coverage of fen area and the drier plant communities (grassland, *S. arctica* snowbed and the heath communities) were about the same at this part of the fen. However, between 1997 and 2007, the continuous fen areas increased whereas the hummocky fen decreased, and the grassland areas increased whereas *S. arctica* snowbed and the heath areas decreased. This indicates wetter conditions in this part of the fen. It is hereby hard to tell if, and how, the plant community composition had changed over the study period. However, Rylekærene is a patterned fen characterized by alternating high, dry heath areas, and low, wet fen areas. These topographic differences result in that no large scale vegetation changes affecting the GPP trend significantly should exist over this short study period.

Despite all the uncertainties discussed, the GPP model captured average field-measured GPP in the study area very well. The LUE-modeled GPP increase was both consistent and substantial, and we consider the generally increasing GPP trend 1992 to 2008 as reliable.

5. Conclusions

By applying a combination of a light use efficiency (LUE)-model and a linear relationship between $FAPAR_{green\_peak}$ and NDVI to incoming PAR and a satellite data set ranging from 1992 to 2008, we show that a substantial increase in peak-growing season GPP has occurred in a high-Arctic wet tundra ecosystem during this period. The average annual increase in peak-growing season GPP between 1992 and 2008 corresponded to 42 mg CO_2 m^{-2} h^{-1} y^{-1}. There was also a strong increase in air temperature (0.15 °C y^{-1}), indicating that the increase in GPP may have been climate-driven. The study demonstrated that NDVI from high-resolution satellite sensors can be used for spatial and temporal extrapolation of $FAPAR_{green\_peak}$ in high-Arctic areas. For this high-Arctic wet tundra ecosystem, the peak growing season LUE (ε_{peak}) was on average 1.63 g CO_2 MJ^{-1}, which is reasonable for high-Arctic ecosystems. Our study also showed that when several models based on field measurements are combined, propagation errors are introduced, which results in considerable model uncertainties. Still, the GPP-model captured field-measured GPP well (RMSE was 192 mg CO_2 m^{-2} h^{-1}). In addition, the study showed that extrapolating FAPAR spatially and temporally and combining it with the LUE-model, can present a useful tool for estimating changes in GPP in wet tundra ecosystems. We conclude that there was a strong increase in LUE-modeled GPP 1992–2008 in Rylekærene, and it was both consistent and substantial.

Acknowledgments

We are thankful to the Swedish research councils, VR and FORMAS for economic support. We are also grateful to the National Environmental Research Institute, Aarhus University, Denmark and personnel at Zackenberg field station for logistic support.

References

ACIA, 2005. Arctic Climate Impact Assessment. Cambridge University Press, New York.
Arndal, M.F., Illeris, L., Michelsen, A., Albert, K., Tamstorf, M.P., Hansen, B.U., 2009. Seasonal variation in gross ecosystem production, plant biomass, and carbon and nitrogen pools in five high Arctic vegetation types. Arctic Antarct. Alpine Res. 41, 164–173.
Bay, C., 1992. A phytogeographical study of the vascular plants of northern Greenland—north of 74° northern latitude. BioScience 36, 3–102.
Bokhorst, S.F., Bjerke, J.W., Tømmervik, H., Callaghan, T.V., Phoenix, G.K., 2009. Winter warming events damage sub-Arctic vegetation: consistent evidence from an experimental manipulation and a natural event. J. Ecol. 97, 1408–1415.
Buus-Hinkler, J., Hansen, B.U., Tamstorf, M.P., Pedersen, S.B., 2006. Snow-vegetation relations in a high Arctic ecosystem: inter-annual variability inferred from new monitoring and modeling concepts. Remote Sens. Environ. 105, 237–247.
Callaghan, T.V., Björn, L.O., Chapin III, F.S., Chernov, Y., Christensen, T.R., Huntley, B., Ims, R.A., Johansson, M., Riedlinger, D.J., Jonasson, S., Matveyeva, N., Oechel, W., Panikov, N., Shaver, G., 2005. Arctic tundra and polar desert ecosystems. In: ACIA (Ed.), Arctic Climate Impact Assessment. Cambridge University Press, New York, pp. 245–352.
Cannell, M., Thornley, J., 1998. Temperature and CO_2 responses of leaf and canopy photosynthesis: A clarification using the non-rectangular hyperbola model of photosynthesis. Ann. Bot. 82, 883–892.
Cappelen, J., 2007. DMI Annual Climate Data Collection 1873–2006, Denmark, The Faroe Islands and Greenland—with graphics and Danish summary. Danish Meteorological Institute, Ministry of Transport and Energy, Copenhagen.
Chander, G., Markham, B.L., Helder, D.L., 2009. Summary of current radiometric calibration coefficients for Landsat MSS, TM, ETM+, and EO-1 ALI sensors. Remote Sens. Environ. 113, 893–903.
Christensen, T.R., Friborg, T., Sommerkorn, M., Kaplan, J., Illeris, L., Soegaard, H., Nordstroem, C., Jonasson, S., 2000. Trace gas exchange in a high-Arctic valley 1. Variations in CO_2 and CH_4 flux between tundra vegetation types. Glob. Biogeochem. Cycles 14, 701–713.
Cook, M.K., Peterson, B.A., Dial, G., Gibson, L., Gerlach, F., Hutchins, K., Kudola, R., Bowen, H.S., 2001. IKONOS technical performance assessment. In: Algorithms for Multispectral, Hyperspectral and Ultraspectral Imagery, vol. VII, pp. 94–108.
Davidson, E.A., Savage, K., Verchot, L.V., Navarro, R., 2002. Minimizing artifacts and biases in chamber-based measurements of soil respiration. Agric. Forest Meteorol. 113, 21–37.
EarthExplorer, 2010. http://earthexplorer.usgs.gov/ (accessed 02/2010).
Falge, E., Baldocchi, D., Olson, R., Anthoni, P., Aubinet, M., Bernhofer, C., Burba, G., Ceulemans, R., Clement, R., Dolman, H., Granier, A., Gross, P., Grunwald, T., Hollinger, D., Jensen, N.O., Katul, G., Keronen, P., Kowalski, A., Lai, C.T., Law, B.E., Meyers, T., Moncrieff, J., Moors, E., Munger, J.W., Pilegaard, K., Rannik, U., Rebmann, C., Suyker, A., Tenhunen, J., Tu, K., Verma, S., Vesala, T., Wilson, K., Wofsy, S., 2001. Gap filling strategies for defensible annual sums of net ecosystem exchange. Agric. Forest Meteorol. 107, 43–69.
Farquhar, G.D., Caemmerer, S., Berry, J.A., 1980. A biochemical model of photosynthetic CO_2 assimilation in leaves of C3 plants. Planta 149, 78–90.
Franke, J., Heinzel, V., Menz, G., 2006. Assessment of NDVI-differences caused by sensor-specific relative spectral response functions. In: 2006 IEEE International Geoscience and Remote Sensing Symposium, vols. 1–8, IEEE, New York, pp. 1138–1141.
GeoBasis, 2010. The Zackenberg Database, http://zdb.dmu.dk (accessed 11/2010).
Goetz, S.J., Prince, S.D., 1996. Remote sensing of net primary production in boreal forest stands. Agric. Forest Meteorol. 78, 149–179.
Gower, S.T., Kucharik, C.J., Norman, J.M., 1999. Direct and Indirect Estimation of Leaf Area Index, fAPAR, and Net Primary Production of Terrestrial Ecosystems—a real or imaginary problem? Remote Sens. Environ. 70, 29–51.
Grøndahl, L., Friborg, T., Christensen, T.R., Ekberg, A., Elberling, B., Illeris, L., Nordstrøm, C., Rennermalm, Å., Sigsgaard, C., Søgaard, H., 2008. Spatial and inter-annual variability of trace gas fluxes in a heterogeneous high-arctic landscape. In: Meltofte, H., Christensen, T.R., Elberling, B., Forchhammer, M.C., Rasch, M. (Eds.), Advances in Ecological Research—High Arctic Ecosystem Dynamics in a Changing Climate. Academic Press, Amsterdam, pp. 473–498.
Huemmrich, K.F., Gamon, J.A., Tweedie, C.E., 2010. Remote sensing of tundra gross ecosystem productivity and light use efficiency under varying temperature and moisture conditions. Remote Sens. Environ. 114, 481–490.
Ito, A., Oikawa, T., 2004. Global mapping of terrestrial primary productivity and light-use efficiency with a process-based model. In: Shiyomi, M., Kawahata, H., Koizumi, H., Tsuda, A., Awaya, Y. (Eds.), Global Environmental Change in the Ocean and on Land. Terrapub, Tokyo, pp. 343–358.
Jia, G.J., Epstein, H.E., Walker, D.A., 2003. Greening of Arctic Alaska, 1981–2001. Geophys. Res. Lett. 30, 1029–1033.
Joabsson, A., Christensen, T.R., 2001. Methane emissions from wetlands and their relationship with vascular plants: an Arctic example. Global Change Biol. 7, 919–932.
La Puma, I.P., Philippi, T.E., Oberbauer, S.F., 2007. Relating NDVI to ecosystem CO_2 exchange patterns in response to season length and soil warming manipulations in Arctic Alaska. Remote Sens. Environ. 109, 225–236.
Lafleur, P.M., Humphreys, E.R., 2007. Spring warming and carbon dioxide exchange over low Arctic tundra in central Canada. Global Change Biol. 14, 740–756.
Mastepanov, M., 2010. Towards a Changed View on Greenhouse Gas Exchange in the Arctic—New Findings and Improved Techniques, PhD thesis, Lund University, Lund.

McGuire, A.D., Anderson, L.G., Christensen, T.R., Dallimore, S., Guo, L., Hayes, D.J., Heimann, M., Lorenson, T.D., Macdonald, R.W., Roulet, N., 2009. Sensitivity of the carbon cycle in the Arctic to climate change. Ecol. Monogr. 79, 523–555.

Meltofte, H., Christensen, T.R., Elberling, B., Forchhammer, M.C., Rasch, M., 2008. Advances in ecological research-high Arctic ecosystem dynamics in a changing climate. Academic Press, Amsterdam.

Monteith, J.L., 1972. Solar radiation and productivity in tropical ecosystems. J. Appl. Ecol. 9, 747–766.

Monteith, J.L., 1977. Climate and the efficiency of crop production in Britain. Philos. T. R. Soc. B. 281, 277–294.

Myneni, R.B., Keeling, C.D., Tucker, C.J., Asrar, G., Nemani, R.R., 1997. Increased plant growth in the northern high latitudes from 1981 to 1991. Nature 386, 698–702.

Myneni, R.B., Williams, D.L., 1994. On the relationship between FAPAR and NDVI. Remote Sens. Environ. 49, 200–211.

Nobrega, S., Grogan, P., 2008. Landscape and ecosystem-level controls on net carbon dioxide exchange along a natural moisture gradient in Canadian low Arctic Tundra. Ecosystems 11, 377–396.

Oechel, W.C., Vourlitis, G.L., Hastings, S.J., Zulueta, R.C., Hinzman, L., Kane, D., 2000. Acclimation of ecosystem CO_2 exchange in the Alaskan Arctic in response to decadal climate warming. Nature 406, 978–981.

ORNL DAAC, 2012. Oak Ridge National Laboratory Distributed Active Archive Center, MODIS subsetted land products, Collection 5. Available on-line from ORNL DAAC, Oak Ridge, Tennessee, USA, http://daac.ornl.gov/MODIS/modis.html.

Parmentier, F.J.W., van Huissteden, J., van der Molen, M.K., Schaepman-Strub, G., Karsanaev, S.A., Maximov, T.C., Dolman, A.J., 2011. Spatial and temporal dynamics in eddy covariance observations of methane fluxes at a tundra site in northeastern Siberia. J. Geophys. Res. 116, G03016.

Ruimy, A., Kergoat, L., Bondeau, A., 1999. Comparing global models of terrestrial net primary productivity (NPP): analysis of differences in light absorption and light-use efficiency. Global Change Biol. 5, 56–64.

Schlesinger, W.H., 1997. Biogeochemistry—An Analysis of Global Change, 2nd edition. Academic Press, Harcourt Brace & Co. Publishers, London, UK.

Schubert, P., Lund, M., Strom, L., Eklundh, L., 2010. Impact of nutrients on peatland GPP estimations using MODIS time series data. Remote Sens. Environ. 114, 2137–2145.

Shaver, G., Street, L.E., Rastetter, E.B., Van Wijk, M.T., Williams, M., 2007. Functional convergence in regulation of net CO_2 flux in heterogeneous tundra landscapes in Alaska and Sweden. J. Ecol. 95, 802–817.

Slayback, D.A., Pinzon, J.E., Los, S.O., Tucker, C.J., 2003. Northern hemisphere photosynthetic trends 1982–99. Global Change Biol. 9, 1–15.

Soegaard, H., Nordstroem, C., 1999. Carbon dioxide exchange in a high-Arctic fen estimated by eddy covariance measurements and modelling. Global Change Biol. 5, 547–562.

Starr, G., Oberbauer, S.F., Ahlquist, L.E., 2008. The photosynthetic response of Alaskan Tundra Plants to Increased Season Length and Soil Warming. Arctic Antarct. Alpine Res. 40, 181–191.

Stow, D., Petersen, A., Hope, A., Engstrom, R., Coulter, L., 2007. Greenness trends of Arctic tundra vegetation in the 1990s: comparison of two NDVI data sets from NOAA AVHRR systems. Int. J. Remote Sens. 28, 4807–4822.

Street, L.E., Shaver, G.R., Williams, M., Van Wijk, M.T., 2007. What is the relationship between changes in canopy leaf area and changes in photosynthetic CO_2 flux in Arctic ecosystems? J. Ecol. 95, 139–150.

Tagesson, T., Lindroth, A., 2007. High soil carbon efflux rates in several ecosystems in southern Sweden. Boreal Environ. Res. 12, 65–80.

Tagesson, T., Mölder, M., Mastepanov, M., Sigsgaard, C., Tamstorf, M.P., Lund, M., Falk, J.M., Lindroth, A., Christensen, T.R., Ström, L., 2012. Land-atmosphere exchange of methane from soil thawing to soil freezing in a high-Arctic wet tundra ecosystem. Global Change Biol. 18, 6, http://dx.doi.org/10.1111/j.1365-2486.2012.02647.

Tans, P., 2009. NOAA/ESRL, www.esrl.noaa.gov/gmd/ccgg/trends (accessed 11/2009).

Tarnocai, C., Canadell, J.G., Schuur, E.A.G., Kuhry, P., Mazhitova, G., Zimov, S., 2009. Soil organic carbon pools in the northern circumpolar permafrost region. Global Biogeochem. Cycles 23, GB2023.

Verbyla, D., 2008. The greening and browning of Alaska based on 1982–2003 satellite data. Global Ecol. Biogeogr. 17, 547–555.

Wania, R., Ross, I., Prentice, I.C., 2009. Integrating peatlands and permafrost into a dynamic global vegetation model: 2. Evaluation and sensitivity of vegetation and carbon cycle processes. Global Biogeochem. Cycles 23, GB3015.

Xu, H., Zhang, T., 2010. Comparison of Landsat-7 ETM+ and ASTER NDVI measurements. In: Remote Sensing of the Environment: The 17th China Conference on Remote Sensing, SPIE, Hangzhou, China, pp. 82030K–82039K.

Zhou, L., Tucker, C.J., Kaufmann, R.K., Slayback, D., Shabanov, N.V., Myneni, R.B., 2001. Variations in northern vegetation activity inferred from satellite data of vegetation index during 1981 to 1999. J. Geophys. Res. 106, 20069–20083.